Preparation of chitosan-loaded zero-valent iron-coated quartz sand and study of its ability to remove Cr(VI) in groundwater

Jianlei Gao, Zixu Zhao, Yixin Yan*, Mengyuan Feng, Yu Wang, Jing Wang

School of Ecology and Environment, Zhengzhou University, Zhengzhou, Henan 450001, China, Tel. +86 13676931078;
emails: yxyan@zzu.edu.cn (Y. Yan), gaojianlei@zzu.edu.cn (J. Gao), zzx11230011@163.com (Z. Zhao),
945968016@qq.com (M. Feng), wy2544428853@163.com (Y. Wang), wangjzzu@126.com (J. Wang)

ABSTRACT

Hexavalent chromium [Cr(VI)] pollution has attracted intense interest in research on heavy metal pollution removal. Here, quartz sand chitosan zero-valent iron (QS-CTS@ZVI) was prepared as a permeable reactive barrier (PRB) medium material by using PRB permeable reaction wall technology and modified CTS-loaded ZVI-coated quartz sand. Characterization analyses were performed with scanning electron microscope, X-ray diffraction, Fourier-transform infrared spectroscopy and thermogravimetry-differential scanning calorimetry. The effects of the reaction time, reaction temperature, initial solution pH, initial Cr(VI) concentration, adsorbent dosage, interfering ions and adsorption cycle on the adsorption of Cr(VI) and total Cr on QS-CTS@ZVI were examined. Then, the adsorption of Cr(VI) by QS-CTS@ZVI was investigated. The results showed that for a ZVI:CTS ratio of 1:1 (m:m), a QS:ZVI ratio of 1:2 (m:m), a pH of 3, t = 5 h, an initial Cr(VI) concentration of 200 mg/L, a QS-CTS@ZVI dosage of 3.5 g/L, and T = 25°C, the efficiencies of Cr(VI) and total Cr removal by QS-CTS@ZVI were 91.6% and 90.9%, respectively. The adsorption efficiency of QS-CTS@ZVI for Cr(VI) was approximately 80% after three reuses. The coexistence of SO_4^{2-} in water can significantly inhibit the Cr(VI) adsorption and removal process. The process of adsorption of Cr(VI) by QS-CTS@ZVI conformed to the pseudo-second-order kinetic equation and the Langmuir adsorption isotherm model.

Keywords: QS-CTS@ZVI composite; Hexavalent chromium; Total Cr; Groundwater

1. Introduction

Chromium (Cr) is a common metal element and is extensively distributed in the Earth's crust [1]. As an important industrial raw material, it is widely used in electroplating, steel, dyeing, leather and other industries [2,3]. Cr is found in many oxidation states in the natural environment, among which the most common and stable forms are Cr(VI) and Cr(III). Compared with Cr(III), Cr(VI) is extremely toxic to organisms and poses a threat to the natural environment [4,5]. In recent years, incidents of Cr(VI) pollution in groundwater have frequently occurred and have strongly impacted local economic production and the social life of individuals [6]. Therefore, technologies and methods for treatment of Cr(VI)-contaminated water, particularly groundwater pollution, must be urgently researched. Permeable reaction wall technology has attracted extensive attention from researchers domestically and abroad because it exhibits good treatment effectiveness, requires few surface treatment facilities and gives rise to very few environmental disturbances [7].

The use of a permeable reactive barrier (PRB) was developed as a novel in situ treatment method for groundwater pollution in the 1990s [8]. Compared with other treatment

* Corresponding author.

methods, the reaction medium in a PRB can separate pollutants from groundwater, provide continuous in situ treatment, create a stable treatment system, and cost-effectively treat various components. It is more competitive and economical for contaminated groundwater remediation [9]. To date, many metals, metalloids and some organic pollutants have been immobilized or effectively degraded by PRBs [10]. Many active media, such as zero-valent iron (ZVI), activated carbon, zeolite, lime and other alkaline materials, have been used in PRBs [11]. Pollutant removal by PRBs mainly occurs in the reaction medium area, which means that the effectiveness of PRBs depends on the type of medium used. However, exploration of suitable dielectric materials is vital for PRBs. Generally, the selection of PRB medium materials is affected by the following aspects: the type, concentration and removal mechanism of the pollutants; repair of the hydrogeological conditions of the regional aquifer; environmental and health impacts; mechanical stability of the PRB and reaction medium (lack of susceptibility to other substances in the groundwater environment); absence of secondary pollution (no release or generation of other contaminants after reaction with contaminants in groundwater); and cost-effectiveness of the material. In addition, in the field application of PRBs, the filling material should ensure an appropriate permeability to avoid changes in groundwater hydrogeology, should be easy to install, and should have reasonable engineering costs. Therefore, a stable, inexpensive and efficient PRB medium material as a medium for removal of Cr(VI) from groundwater must be found. Domestic and foreign researchers have extensively investigated PRB technology, particularly PRB fillers. ZVI-based PRBs have been shown to have great potential in the treatment of various inorganic and organic pollutants [12–16].

Zero-valent iron (ZVI) has the advantages of a high reaction rate, a large specific surface area and high reduction activity and can be applied in engineering practice [17,18]. However, continuous exposure of ZVI active sites causes the material to be easily reoxidized during use; thus, the material loses its good reusability and antioxidant properties. A PRB reactor suffers from severe blockage when ZVI powder is used alone. To solve these problems and reduce the preparation cost of adsorption materials, a stable and inexpensive natural inorganic material must be selected as a carrier to support iron powder, disperse dense iron powder and increase the reaction contact area. Using inexpensive and readily available quartz sand as a skeleton can effectively improve the dispersion and permeability of iron powder. However, if quartz sand and iron powder are directly mixed, then iron powder is unevenly dispersed, resulting in a poor removal effect. Therefore, a coating material on quartz sand should be prepared by modifying iron powder to achieve efficient Cr removal.

Researchers have studied the removal effect of ZVI-loaded bentonite, biochar and chitosan (CTS) in the removal of hexavalent Cr pollution in groundwater [19–21]. They found that coating of CTS on the surface of ZVI powder helped reduce the degree of ZVI oxidation and enhance the adsorption performance. Chitosan (CTS) has a large number of basic amino ($-NH_2$) groups on the surface, and the nitrogen atom easily combines with H^+, causing CTS to have an overall positive charge; therefore, CTS exhibits

excellent performance for cation flocculation. Some experiments showed that the maximum Cr(VI) reduction rate of CTS-stabilized ZVI was approximately three times that of ZVI alone [22]. Natural CTS is easily protonated in acidic solution, and the free $-NH_2$ that forms causes the heavy metals to lose their coordination ability, directly affecting the adsorption of heavy metals on CTS [23,24]. The linear chain structure of CTS has been changed into a network structure by cross-linking with epichlorohydrin, improving the chemical stability, mechanical strength and heavy metal adsorption on the CTS adsorbent [25]. However, cross-linking is disadvantageous in that the cross-linking process causes some active groups on CTS molecules to be occupied, resulting in a reduction in the number of active adsorption sites on CTS that adsorb heavy metals. Copolymerization of CTS with acrylic acid expands the number and type of functional groups of CTS [26], enhancing the adsorption of Cr(VI) by CTS [27–29]. In addition, such copolymers are biodegradable and can reduce the generation of secondary waste [30].

In this study, epichlorohydrin and acrylic acid-modified CTS were used as basic organics to combine with ZVI to produce a CTS-modified ZVI mixture that was coated on the surface of quartz sand acting as a substrate. The coating material can strengthen the material dispersion, improve the utilization efficiency, extend the service life, and achieve good removal of Cr(VI) and total Cr. The surface morphology, structure composition, surface chemical properties and thermal stability were analyzed by scanning electron microscope (SEM), X-ray diffraction (XRD), Fourier-transform infrared spectroscopy (FTIR) and thermogravimetry-differential scanning calorimetry (TG-DSC). The effects of the reaction time, reaction temperature, initial solution pH, initial Cr(VI) concentration, adsorbent dosage, interfering ions and adsorption cycle on the Cr(VI) and total Cr adsorption properties were investigated. Finally, the Cr(VI) and total Cr adsorption mechanism was analyzed by combining the isotherm model and kinetic models of adsorption. This study provides guidance for the design of PRB media for removal of Cr(VI) and total Cr in groundwater.

2. Materials and methods

2.1. Materials

Hydrochloric acid (HCl), nitric acid (HNO$_3$) and sulfuric acid (H$_2$SO$_4$) were purchased from Luoyang Haohua Chemical Reagent Co., Ltd., and phosphoric acid (H$_3$PO$_4$), sodium hydroxide (NaOH), acrylic acid (C$_3$H$_4$O$_2$), glacial acetic acid (CH$_3$COOH), and epichlorohydrin (C$_3$H$_5$ClO) were purchased from Tianjin Komeo Europe Chemical Test Co., Ltd. ZVI powder (ZVI) was purchased from Tianjin Komeo Chemical Reagent Co., Ltd., CTS (C$_{56}$H$_{103}$N$_9$O$_{39}$) was purchased from Shanghai Aladdin Biochemical Technology Co., Ltd., and diphenylcarbazide (C$_{13}$H$_{14}$N$_4$O) was purchased from Tianjin Damao Chemical Reagent Factory. Potassium dichromate (K$_2$Cr$_2$O$_7$) was purchased from Tianjin Fengchuan Chemical Reagent Co., Ltd., and quartz sand was purchased from Zhengzhou. All chemicals use analytical reagent preparation of the quartz sand chitosan zero-valent iron (QS-CTS@ZVI) composite

The quartz sand passed through the 35 mesh sieve to ensure that the particle size of the quartz sand was 0.5 mm. The quartz sand was washed multiple times with ultra-pure water until the water was clear. After filtering out the quartz sand, it was dumped in a surface dish. The samples were placed in a blast drying oven, dried at a constant temperature of 105°C for 12 h, and stored in a self-sealing bag for further use. At room temperature, CTS (0.2 g) was added to 2% acetic acid (10 mL). The solution was stirred at 2,000 rpm for 30 min until CTS had completely dissolved into a slightly yellow transparent solution. Quartz sand (0.4 g) was mixed into the CTS solution, the mixture was stirred at 2,000 rpm for 1 h, and acrylic acid (AA, 0.2 mL) was added. Then, stirring at 2,000 rpm was performed for 1 h, and epichlorohydrin (EPI, 0.2 mL) was added and stirred at 2,000 rpm for 3 h. After 5 h of reaction, a $CuSO_4 \cdot 5H_2O$ solution (0.4 mL, 10 g/L) was added. After the solution was evenly stirred, nitrogen was added, and ZVI powder (0.2 g) was weighed and added (ratio of ZVI powder to CTS of 1:1) to the mixed solution under anaerobic conditions. After 10 min of stirring, 2 mol/L NaOH was dropwise added and continuously stirred. At this time, the mixed solution gradually agglutinates from a paste into a micelle until the SA-CTS mixed adsorbent solution in the beaker was clear and transparent. The aggregates were immersed in the solution. After 12 h, the residual NaOH was repeatedly washed with deionized water to eliminate the alkalinity of the solution, After vacuum drying at 60°C, the quartz sand-loaded chitosan adsorbent was obtained after crushing and sieving, which was recorded as QS-CTS@ZVI.

2.2. Characterization

The samples in this study were determined to be QS-CTS@ZVI using a Quanta 200 environmental scanning electron microscope. The samples were evenly spread on the sample table of the scanning electron microscope and sprayed with gold. The particle sizes and microstructures of the three materials were observed and photographed under an acceleration voltage of 3 kV. QS-CTS@ZVI was examined using an XRD-6100 XRD analyzer (Shimadzu, Japan). The scanning range was 5–90°. The crystal structures of the three materials were examined at a scanning rate of 10°/min. A Nicolet iS50 Fourier transform infrared spectrometer was used to examine QS-CTS@ZVI, and the molecular vibration–rotation energy level transitions formed a specific infrared absorption spectrum. The functional groups in the three materials before and after coating were evaluated, the structures of the materials were analyzed, and the adsorption mechanism was explored based on the comparison of the obtained infrared spectra. In this study, QS-CTS@ZVI (10 mg) was weighed and placed in an alumina crucible, and the heating rate was set at 10°C/min. The rate of QS-CTS@ZVI weight loss was tested in the temperature range of 30–1,000°C, and the curve of the coating material quantity vs. temperature was plotted.

2.3. Experiments of adsorption of Cr(VI) by the QS-CTS@ZVI composite

A potassium dichromate ($K_2Cr_2O_7$) stock solution with a Cr(VI) concentration of 1,000 mg/L was prepared. During the experiment, the stock solution of Cr(VI) was diluted to the required concentration. QS-CTS@ZVI was added to the Cr(VI) standard solution (10 mL) diluted to the required concentration in a centrifuge tube, and 0.1 mol/L HCl solution was used to adjust the pH of the reaction system. Then, batch experiments were carried out to investigate the effects of the reaction time, adsorbent concentration, adsorbent dosage, reaction temperature, coexisting ions, and initial solution pH on the Cr(VI) adsorption performance of the composites. The centrifuge tube was placed at 298 K, and the constant temperature shaker was vibrated for 480 min at a speed of 150 rpm. The reaction solution was aspirated by a 20 mL syringe and filtered through a 0.45 μm micro-porous membrane. The Cr(VI) concentration was measured after dilution for specific times. After the adsorption experiment, the residual Cr(VI) content in the solution was determined by diphenylcarbazide spectrophotometry.

$$Q_e = \frac{V(C_0 - C_e)}{m} \quad (1)$$

$$Q_t = \frac{V(C_0 - C_t)}{m} \quad (2)$$

$$\%Removal = \frac{100(C_e - C_0)}{C_0} \quad (3)$$

where q_t (mg/g) is the Cr(VI) adsorption capacity at time t. q_e (mg/g) is the Cr(VI) adsorption capacity at equilibrium. V (L) is the solution volume. m (g) is the adsorbent weight. C_0, C_t, and C_e (mg/L) are the initial solution concentration, concentration at time t, and final concentration, respectively.

To describe the adsorption mechanism and related reaction rate of Cr, the experimental data were linearly simulated by the intraparticle diffusion model and first-order kinetic and quasi-second-order kinetic models.

The intraparticle diffusion model of Weber and Morris is described by the empirical expression shown in Eq. (4) [31].

$$Q_t = k_{id}t^{1/2} + C_i \quad (4)$$

where k_{id} (mg/(g·min)) is the rate constant of the intraparticle diffusion model. q_t (mg/g) is the adsorption capacity of the adsorbent for Cr(VI) ions at t min. t (min) is the reaction time. C_i (mg/g) is the intercept.

The first-order reaction kinetic model is as follows:

$$\ln(q_e - q_t) = \ln q_e - k_1 t \quad (5)$$

where k_1 (g/(mg·min)) is the pseudo-first-order rate constant. q_t (mg/g) is the adsorption capacity of the adsorbent for heavy metal ions Cr(VI) at t min, which was calculated. q_e (mg/g) is the adsorption capacity of Cr(VI) in mg/g when the adsorption reaction reaches equilibrium. t (min) is the reaction time.

The pseudo-second-order kinetic model is given by Eq. (6):

$$\frac{t}{q_t} = \frac{1}{k_2 q_e^2} + \frac{t}{q_e} \quad (6)$$

where k_2 (g/(mg·min)) is the rate constant of the pseudo-second-order reaction.

After the adsorption between the material and the adsorbate in the solution reached equilibrium at a certain temperature, Langmuir and Freundlich adsorption isotherm models were used to fit the adsorption behavior of the solid–liquid system, and the mechanism in the reaction process was discussed.

- Langmuir adsorption isotherm model

The Langmuir model assumes that the adsorbent surface is uniform, and the adsorbate undergoes single-molecule adsorption on the adsorbent surface. The Langmuir model is described by Eq. (7).

$$\frac{c_e}{q_e} = \frac{1}{q_{max}K_L} + \frac{c_e}{q_{max}} \tag{7}$$

where q_e (mg/g) is the adsorption amount on the adsorbent. q_{max} (mg/g) theoretically represents the maximum adsorption capacity per unit mass of the adsorbent. c_e (mg/L) is the residual Cr(VI) ion concentration in the solution when the adsorption reaches equilibrium. K_L (L/mg) is a Langmuir constant and represents the binding ability of the active site of the adsorbent and Cr(VI) ions.

- Freundlich adsorption isotherm model

The Freundlich adsorption isotherm model is an empirical model that is suitable for describing multilayer adsorption of surface heterogeneous adsorbents. The isothermal adsorption equation is shown in Eq. (8).

$$\lg q_e = \lg K_F + \frac{1}{n}\lg c_e \tag{8}$$

where K_F ($mg^{1-1/n}·L^{1/n}$) is the Freundlich constant representing the adsorption capacity of the adsorbent for Cr(VI) ions, and $1/n$ is the strength of binding between the Cr(VI) adsorbate and adsorbent.

2.4. Cyclic adsorption experiment

The adsorbed QS-CTS@ZVI was placed in 0.1 mol/L NaOH solution. At 25°C, the rotation speed of the constant temperature shaker was set to 150 rpm, and the solution was extracted and examined after shaking for 180 min. Then, QS-CTS@ZVI was filtered and cleaned with deionized water until the pH of the cleaning solution was close to neutral, and the regenerated adsorbent was prepared after drying in a vacuum oven. The performance of regenerated adsorbents was tested under the same single-factor experiment.

3. Results and discussion

3.1. Characterization

3.1.1. SEM results

The surface of quartz sand (QS) (Fig. 2a) is smooth and flat with a small number of holes. As a result, QS has extremely low adsorption performance (Fig. 2b). The surface of QS-CTS@ZVI is flocculent, which increases the specific surface area of the adsorbent material, provides sufficient adsorption space, and promotes full contact between ZVI and Cr(VI), promoting adsorption and reduction of Cr(VI). Abundant sites for efficient removal are provided. The surface pore structure essentially disappears, indicating that QS is completely covered by the mixture of ZVI and CTS. For the ZVI particles with an irregular surface attachment morphology, most of the ZVI particles have sizes in the 80–160 nm range, and a small amount of agglomerated ZVI particles have sizes in the 280–830 nm range.

3.1.2. XRD results

Fig. 2c shows the XRD pattern of the original quartz sand. A strong diffraction peak is clearly present at $2\theta = 26.7°$, corresponding to SiO_2. In the diffraction pattern of quartz sand, SiO_2 diffraction peaks are present at $2\theta = 39.5°$, 40.4°, 67.7° and 68.4°, but these diffraction peaks become weak or disappear in the coated material. This may be because the surface of the coated sample is coated by a large number of organic substances. The quartz sand in the material is essentially fully covered by organic substances and cannot be detected by XRD. In the process of preparing the materials, the chemical bonds and the original molecular structure of CTS may be damaged, resulting in a decrease in the crystallinity of CTS. No evident diffraction peak of CTS is observed in QS-CTS@ZVI, possibly because the structure of the CTS molecular chain in this material is damaged, the binding force between hydrogen bonds is weakened, and the structure is disordered, resulting
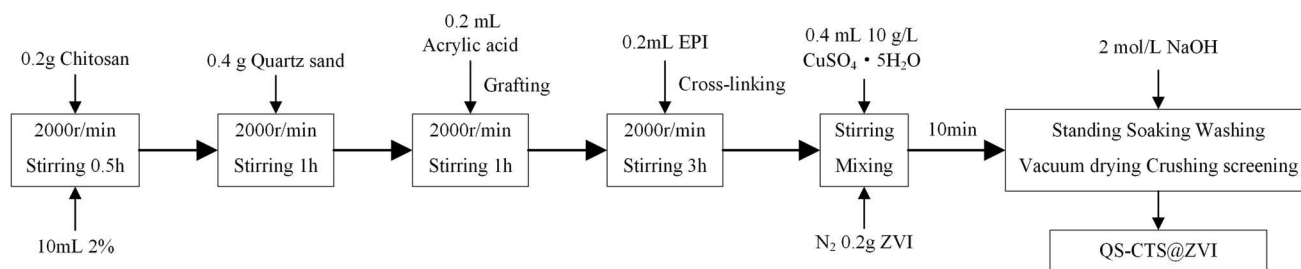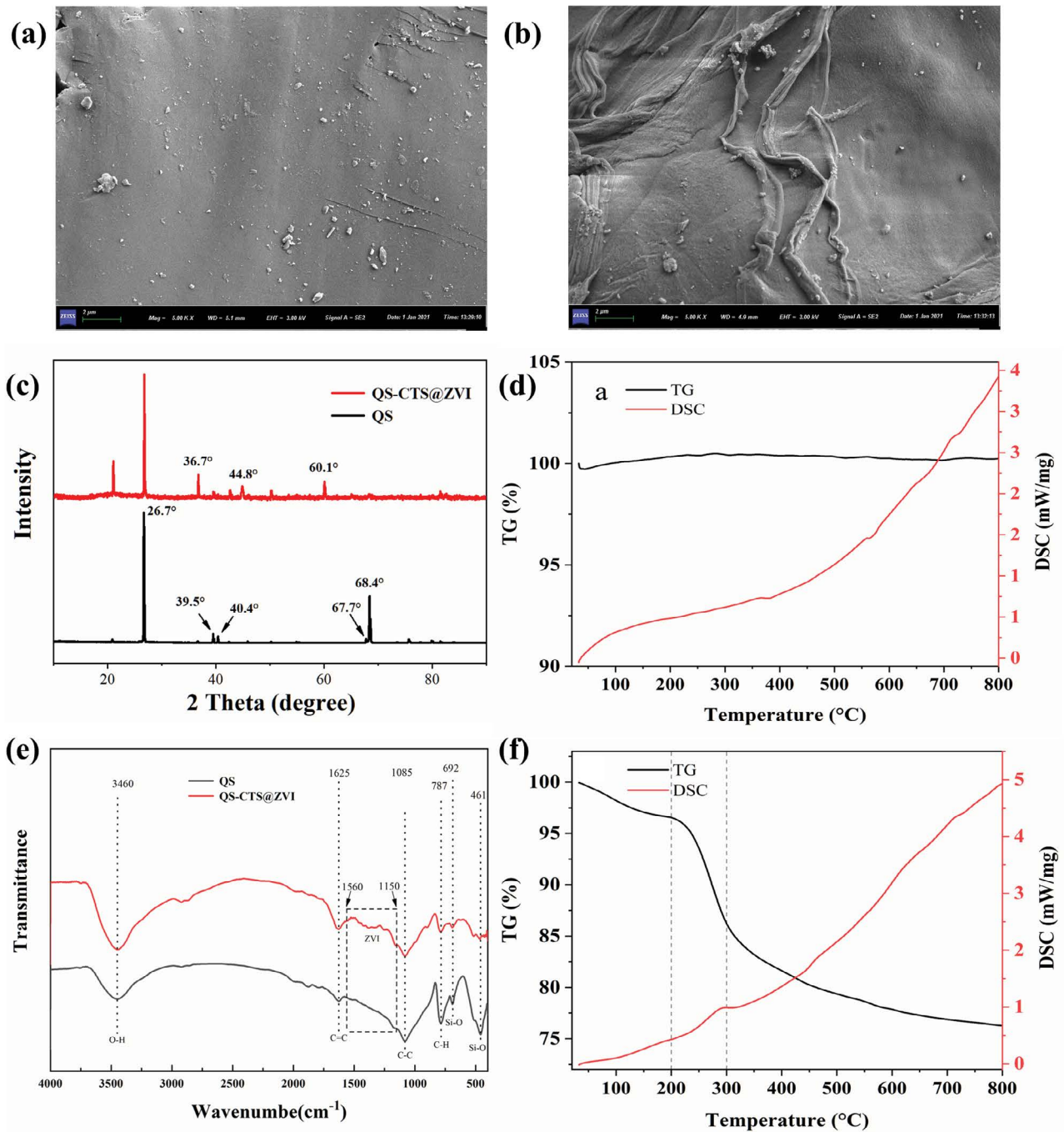

Fig. 1. QS-CTS@ZVI production flow chart.

Fig. 2. SEM images of the original quartz sand (a) ×5,000 and QS-CTS@ZVI (b) ×5,000, (c) XRD pattern, (e) FTIR spectra, and TG-DSC change curves (d) quartz sand and (f) QS-CTS@ZVI.

in decreased crystallinity [32]. This disordered morphology is beneficial for the adsorption and removal efficiency.

Diffraction peaks of ZVI appear at $2\theta = 44.8°$ and $60.1°$ in the QS-CTS@ZVI XRD pattern, demonstrating that ZVI powder has been successfully loaded on QS-CTS@ZVI, but other weak peaks are also observed for QS-CTS@ZVI, such as the diffraction peak at $2\theta = 36.7°$. However, a small deviation is observed, possibly due to the oxidation of Fe(0) to Fe(III) and Fe(II), so the larger Fe(III) or Fe(II) ion replaced

the smaller Fe(0) ion [33]. The experimental results also show that a small amount of oxidized ZVI on the surface of the material has little effect on the removal of Cr(VI).

3.1.3. FTIR results

Fig. 2e shows the FTIR spectra of the original sample and the coated material. The quartz sand is mainly composed of SiO_2 mineral materials and is Si-rich; the peaks

at 692 and 461 cm^{-1} are due to the stretching vibration of the Si−O bonds in quartz sand. There are Si−O−Si and Si−O chemical bonds in QS-CTS@ZVI, verifying that QS-CTS@ZVI is coated with quartz sand acting as a substrate material. The absorption peaks at 1,085 and 787 cm^{-1} correspond to the C−C and C−H vibrations, respectively. The spectrum significantly changes in the 1,560–1,150 cm^{-1} region, indicating that ZVI particles are immobilized on QS [34]. The peak at 1,625 cm^{-1} is the C=C stretching vibration peak, and the QS-CTS@ZVI peak shows that acrylic acid was successfully grafted on QS-CTS@ZVI. The original quartz sand and QS-CTS@ZVI have an absorption peak at 3,460 cm^{-1}, corresponding to the −OH stretching vibration [35]. The peak abruptly rises here, possibly due to superposition of the −NH and −OH peaks in QS-CTS@ZVI under the combined action of the −NH and −OH stretching vibrations in the original peak, resulting in the increase in the peak; this indicates that the −NH of CTS is still in excess. CTS molecules undergo a cross-linking reaction, and the absorption band near 1,625 cm^{-1} is due to the first and second amide groups [36]. The changes in the height and width of the absorption peak discussed here indicate that the material was successfully loaded with CTS.

3.1.4. Thermogravimetry-differential scanning calorimetry results

In a N$_2$ atmosphere, the temperature was changed from 100°C to 1,000°C at a rate of 10°C/min. The organic matter content in quartz sand and QS-CTS@ZVI was determined by thermogravimetric analysis, and the results are shown in Fig. 2d and f. Quartz sand in this temperature range shows almost no weight change and is relatively stable. Comparing the results in Fig. 2f the QS-CTS@ZVI coating material shows a strong weight loss. In Fig. 2f, an exothermic peak is present near 300°C in the differential scanning calorimetry (DSC) curve that may be due to a thermal cross-linking reaction during heat treatment that leads to the formation of a new polymer. The secondary depolymerization of this polymer in the N$_2$ atmosphere leads to the exothermic behavior observed in the DSC curve [37].

Fig. 2f shows that there are three weight loss stages. In the first weight loss stage, in the temperature range of 30°C–200°C, the adsorbed water and crystal water on the surface of QS-CTS@ZVI evaporate, resulting in a certain degree of weight loss, whereas QS-CTS@ZVI does not show evident weight loss at this stage. For QS-CTS@ZVI, a small amount of copper sulfate pentahydrate solution was added during the preparation, and copper sulfate pentahydrate loses two crystal water molecules at 65°C and 90°C [38]. At 100°C, the weight loss rate of QS-CTS@ZVI remains within 2%, indicating that QS-CTS@ZVI maintains good thermal stability in the application temperature range of the PRB.

In the second-stage, the weight loss rate of QS-CTS@ZVI is high in the temperature range from 200°C to 300°C. CTS is very stable due to the action of macromolecular hydrogen bonds and begins to decompose only above 200°C. The decomposed CTS is further lysed, producing small molecular volatile products, by random chain reaction and carbonization [39]. The weight loss rate of QS-CTS@ZVI is 10.4% in this temperature range.

At temperatures less than 300°C, CTS cannot be completely decomposed in a short time [40]. In the third stage at 300°C–800°C, the ZVI powder loaded on QS-CTS@ZVI does not decompose at high temperatures, and no other substances are produced. Therefore, above 300°C, the quartz sand on the surface decomposes, and the weight loss rate is 9.9%. The loaded CTS is concluded to account for 10.4% of the total weight of the material, the organic matter on the surface of quartz sand accounts for 9.9% of the total weight of the material, the crystal water lost by heating of copper sulfate pentahydrate accounts for approximately 2% of the total weight, and the remaining material accounting for approximately 77.7% of the total weight is quartz sand, ZVI and a small amount of copper oxide.

3.2. Experimental results of batch adsorption of Cr(VI)

3.2.1. Adsorption kinetic studies

The ratio of the added ZVI and CTS in the material is 1:1. If CTS does not completely encapsulate ZVI, then the bare ZVI on the material reflects the initial stage of Cr(VI) oxidation to Cr(III). At this time, the Cr(III) concentration in water rapidly increases, and the amount of total Cr removal decreases. However, Fig. 3a and b show that the trends of adsorption of Cr(VI) and total Cr on QS-CTS@ZVI are similar. At the initial reaction stage, the equilibrium amount of total Cr adsorption rapidly increases, and the concentration of Cr(III) is relatively low; thus, Cr(VI) is not reduced to Cr(III) prior to being adsorbed by CTS. ZVI in the material is concluded to be essentially wrapped by CTS, and there is almost no ZVI exposed on the surface of the material. The adsorption rate for Cr(VI) and total Cr by QS-CTS@ZVI is higher at a reaction time of 0−60 min and then gradually decreases after the reaction time reaches 60 min. At 60 min, the adsorption capacity of QS-CTS@ZVI for Cr(VI) exceeds 80% of the equilibrium adsorption capacity. Thus, adsorption of Cr(VI) and total Cr by QS-CTS@ZVI is divided into two stages: a fast adsorption stage and a slow adsorption stage [4].

In the fast adsorption stage, QS-CTS@ZVI first adsorbs Cr(VI) on the surface of the material via electrostatic interactions through its abundant active sites, and the reaction is faster in this stage. In the slow adsorption stage, the ZVI powder contained in QS-CTS@ZVI reduces the Cr(VI) adsorbed on its surface to Cr(III) through its own electron transfer activity under acidic conditions. Therefore, the amount of Cr(VI) removed is still significantly increased, but Cr(III) is not completely adsorbed by QS-CTS@ZVI, resulting in a lower adsorption for total Cr than Cr(VI). When the reaction time is further prolonged, the amount of QS-CTS@ZVI adsorption changes very little, indicating that QS-CTS@ZVI is in the stage of adsorption saturation under these conditions.

Fig. 4a and b show the linear fitting of the reaction time t with $\ln(q_e - q_t)$ and c_t/q_e as the ordinates, respectively. The kinetics of Cr(VI) removal by QS-CTS@ZVI were analyzed. Fig. 4a and b indicate that under three different initial concentrations, compared with the first-order kinetic equation ($R^2 \leq 0.97$), the removal of Cr(VI) by QS-CTS@ZVI is more consistent with the second-order kinetic equation

($R^2 \geq 0.99$). The adsorption process of QS-CTS@ZVI is mainly surface adsorption [41,42]. Cr(VI) has a passivation effect on ZVI powder, and a passivation layer of $Cr_{0.667}ZVI_{0.333}OOH$ or $Cr_{0.667}ZVI_{0.333}(OH)_3$ can be formed on the surface of QS-CTS@ZVI to prevent electron transfer between the internal and external ZVI powder so that the adsorption rate will decrease [43,44].

Fig. 4c clearly shows that QS-CTS@ZVI data can be fitted by three straight lines at different initial concentrations. This result is consistent with adsorption process that can be divided into the following stages: surface diffusion, internal diffusion and adsorption reaction [45]. In the first stage of adsorption, Cr(VI) quickly occupies the active sites on the QS-CTS@ZVI surface, and the reaction time is the shortest in this stage [46]. In the second-stage, as shown in Table S1, the C_i of the material first increases and then decreases, indicating that the influence of the boundary layer on the adsorption efficiency first increases and then decreases. At the beginning of the reaction, a large number of Cr(VI) ions are present in

the reaction system. These ions quickly establish a layer of a Cr(VI) ion film on the surface of QS-CTS@ZVI, preventing the coating material from contacting other Cr(VI) ions. In the subsequent reaction, Cr(VI) ions must overcome the influence of the boundary effect on adsorption. In the third stage, the adsorbed Cr(VI) ions diffuse inside QS-CTS@ZVI and react with internal functional groups. These three stages show that the decisive factors for the adsorption rate of QS-CTS@ZVI are surface diffusion and intraparticle diffusion. In addition, no fitting line in Fig. 4c passes through the coordinate origin, and this result once again confirms that intraparticle diffusion is not the only rate-controlling step for these three adsorption materials [47].

3.2.2. Adsorption isotherms

With 200 mg/L as the initial concentration, the adsorption process of QS-CTS@ZVI on Cr(VI) was explored at different temperatures (293, 298, and 303 K), and the Langmuir
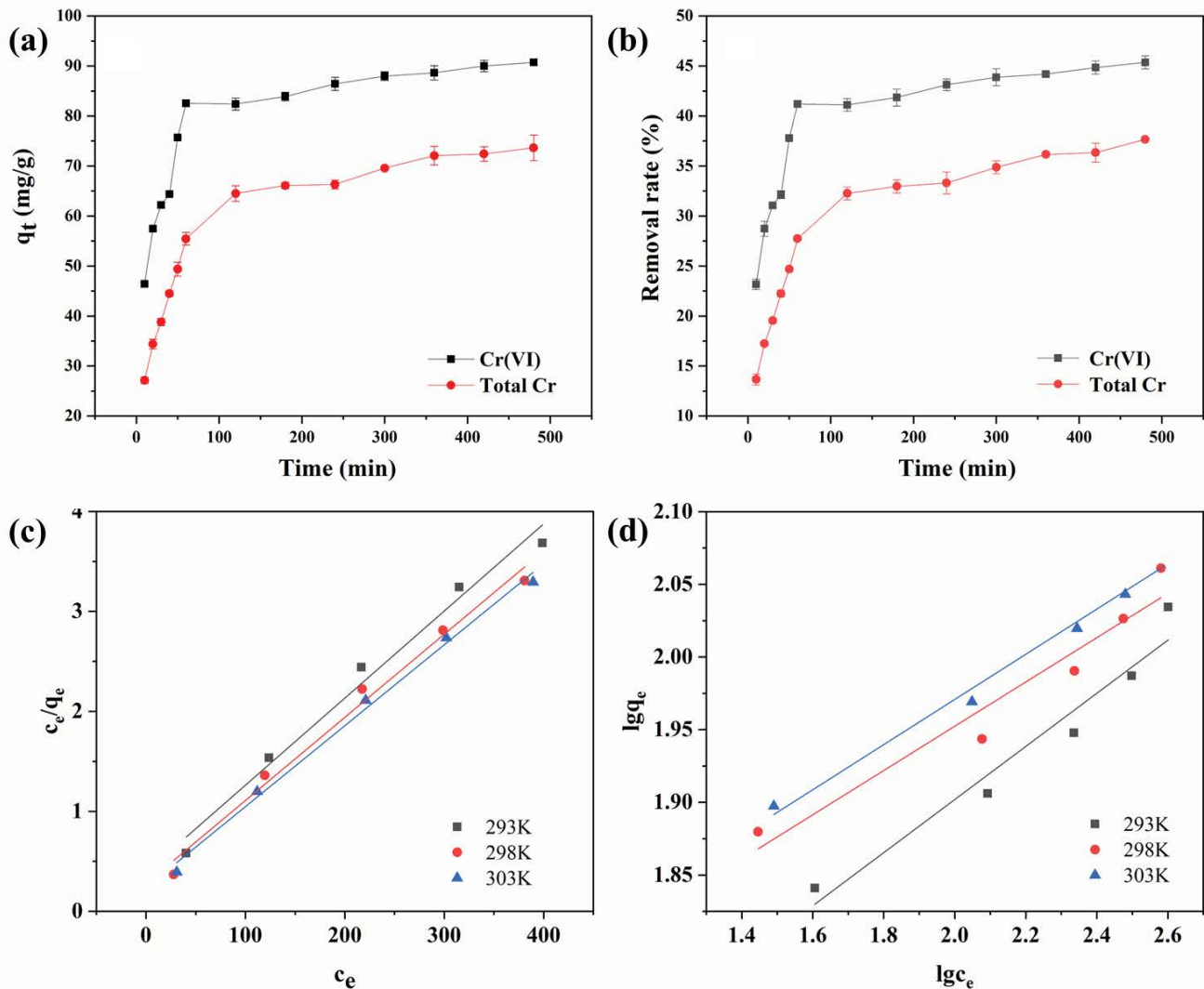

Fig. 3. Effect of time on the (a) equilibrium adsorption capacity and (b) rates of Cr(VI) and total Cr removal by QS-CTS@ZVI; QS-CTS@ZVI (adsorption conditions: pH 3, dosage 0.01 g, 25°C, 200 mg/L) (c) Langmuir isotherm model fitting and (d) Freundlich isotherm model fitting.
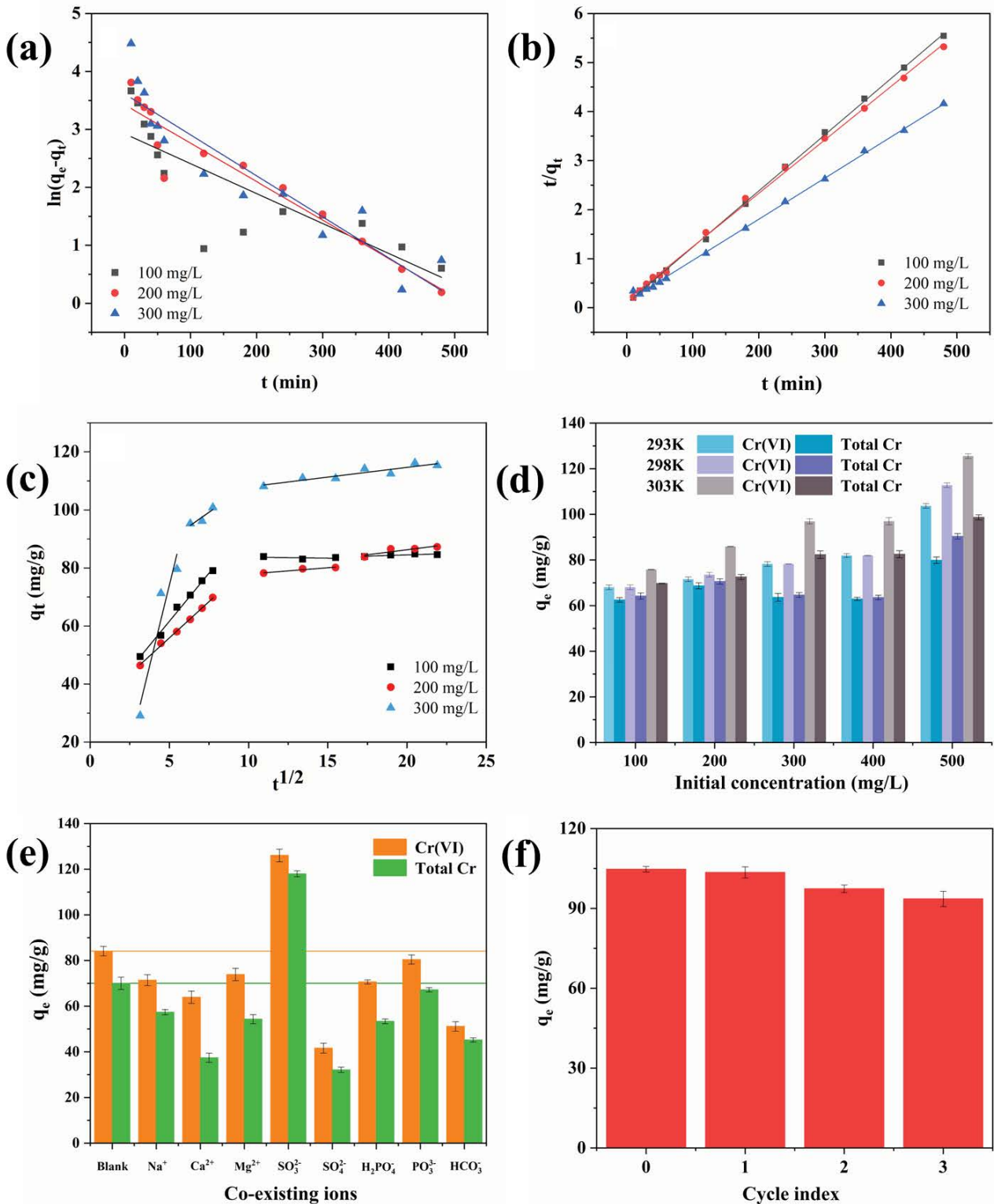
Fig. 4. Fitting of QS-CTS@ZVI kinetics: (a) quasi-first-order kinetics, (b) quasi-second-order kinetics, (c) curve of the intraparticle diffusion model, (d) effect of temperature on Cr(VI) and total Cr removal by QS-CTS@ZVI (adsorption conditions: pH 3, 200 mg/L, dosage 0.01 g, 5 h), (e) effect of coexisting ions on Cr(VI) and total Cr removal by QS-CTS@ZVI (adsorption conditions: pH 3, dosage 0.01 g, 25°C, 5 h, 200 mg/L, 0.1 mL 1 mol/L coexisting ions) and (f) adsorption properties of QS-CTS@ZVI for Cr(VI) after analysis (adsorption conditions: pH 3, dosage 0.01 g, 25°C, 5 h, initial concentration 200 mg/L).

model and Freundlich model were used to fit the process (Fig. 3c and d). The fitting parameters are shown in Table S3. The theoretical adsorption capacities (114.8, 120.3, and 123.6 mg/g) were calculated by Langmuir model fitting and were found to increase to varying degrees, indicating that an increase in the temperature was beneficial for Cr(VI) removal by QS-CTS@ZVI. The constant K is derived from Freundlich theory and decreases with increasing temperature, confirming good adsorption during the process at lower temperatures. In addition, when $1/n$ is between 0 and 1 and n is greater than 1, all conditions are conducive to the adsorption of Cr(VI). The correlation coefficients R^2 of the Langmuir model are 0.98, 0.99 and 0.99, and the correlation coefficients R^2 of the Freundlich model are 0.95, 0.94 and 0.99, respectively, indicating that the Langmuir isotherm is more suitable than the Freundlich isotherm. In a study on the adsorption of Cr(VI) in water by CTS-coated fly ash composites, Wen et al. also found that compared to the Freundlich isotherm, the Langmuir isotherm was more suitable for fitting the adsorption process of Cr(VI) [48].

3.3. Effect of temperature

Fig. 4c shows that with the change in the temperature (293–303 K), the adsorption capacity of QS-CTS@ZVI for Cr(VI) and total Cr increases, indicating that heating is beneficial for the adsorption process of QS-CTS@ZVI and that this reaction is an endothermic reaction. At three temperatures, the adsorption capacity of QS-CTS@ZVI for Cr(VI) is higher than that for total Cr. At the same initial concentration, the QS-CTS@ZVI adsorption amount weakly increases with the change in the temperature [49]. Under the set conditions, QS-CTS@ZVI may tend to be saturated, and its adsorption amount will then reach equilibrium. In this case, the improvement in the adsorption effect by changing the temperature will not be evident.

3.4. Effect of pH

The pH of the reaction system has a strong influence on the process of Cr(VI) adsorption by QS-CTS@ZVI. Fig. 5a and b show the adsorption capacity and adsorption efficiency changes for Cr(VI) and Cr adsorption by QS-CTS@ZVI as the pH of the solution varies from 3 to 8. With increasing pH, the Cr(VI) and total Cr removal rates gradually decrease from approximately 40% to less than 10%. This is mainly because Cr(VI) exists in the solution mostly in the form of $HCrO_4^-$ and $Cr_2O_7^{2-}$ under acidic conditions, and the lower pH increases the degree of CTS protonation. A large amount of H^+ binds to the surface of CTS, enhancing the electrostatic attraction between CTS and $HCrO_4^-$ as well as $Cr_2O_7^{2-}$, which in turn improves the adsorption efficiency of QS-CTS@ZVI [50,51]. Moreover, the corrosion of ZVI powder is accelerated under acidic conditions, and the ferrochromium hydrate precipitates produced by the reaction are also reduced (as shown in Eq. (9)). ZVI powder has high activity, but compared with other valence iron ions, ZVI powder is more prone to oxidation reactions. When ZVI powder is in contact with air, it can be oxidized to Fe_3O_4 and coated on the surface of QS-CTS@ ZVI, and the adsorption capacity of oxidized QS-CTS@

ZVI will be greatly reduced. However, in the presence of a greater amount of H^+ in the solution, QS-CTS@ZVI reacts with H^+, as shown in Eq. (10). The oxide layer on the surface of QS-CTS@ZVI is decomposed into Fe(III), and reduced Fe(II) promotes the adsorption and reduction of Cr(VI) by QS-CTS@ZVI; thus, the adsorption capacity for Cr(VI) and total Cr is higher under low pH conditions. With increasing pH, the oxide layer does not decompose in an alkaline environment. Instead, OH^- promotes the production of a passivation layer on the surface of ZVI powder. The passivation layer hinders the interaction of QS-CTS@ZVI and Cr(VI). In this environment, Cr(VI) mainly exists in the solution as CrO_4^{2-}. The electrostatic attraction between CrO_4^{2-} and the positively charged CTS is weakened, and more OH^- competes for adsorption, reducing Cr(VI) adsorption. The lower adsorption capacity also hinders the removal of total Cr. Total Cr removal is divided into Cr(VI) and Cr(III) adsorption. The adsorption of Cr(VI) becomes more favorable with stronger acidity; however, acidity is not conducive to the adsorption of Cr(III). When the system is neutral and alkaline, Cr(VI) is not easily reduced. In this case, an electrostatic repulsion exists between Cr(VI) and the adsorbent that inhibits adsorption. Therefore, QS-CTS@ ZVI has a significantly higher Cr(III) removal rate under acidic conditions than under alkaline conditions [52,53].

$$Fe^0 + CrO_4^{2-} + 4H_2O \rightarrow Cr(OH)_3 + 2OH- \tag{9}$$

$$Fe_3O_4 + 8H^+ \rightarrow Fe^{2+} + 2Fe^{3+} 4H_2O \tag{10}$$
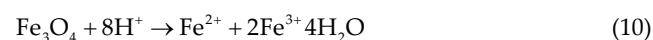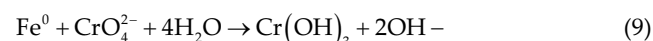
3.5. Effect of the initial Cr(VI) concentration

Fig. 5c shows that with increasing Cr(VI) concentration, the amounts of Cr(VI) and total Cr adsorption by QS-CTS@ ZVI gradually increase, with similar adsorption trends. More Cr(VI) is provided with the increased initial concentration, and the total Cr content increases, increasing the likelihood of molecular collisions between QS-CTS@ZVI, Cr(VI) and Cr(III). CTS increases the adsorption sites for Cr(VI), thereby enhancing the adsorption capacity of the composite material for Cr(VI). Fig. 5d shows that when the concentration of Cr(VI) is 10 mg/L, more than 99% of Cr(VI) in the solution can be removed by QS-CTS@ZVI, and the removal rate of total Cr reaches 80%. As the concentration increases, the rate of Cr(VI) removal by QS-CTS@ ZVI decreases, which is related to the number of active sites in QS-CTS@ZVI. An increasing amount of Cr(VI) will cause more active adsorption sites to be occupied, and the quantity of the adsorbent added to the solution is limited; this results in more Cr(VI) that cannot be combined with active sites, adsorption saturation of QS-CTS@ZVI, the inability to remove Cr(VI) in the solution, and a decrease in the removal rate. According to Fig. 5c and d, when the initial concentration increases from 10 to 100 mg/L, the adsorption capacity of QS-CTS@ZVI for Cr(VI) rapidly increases from 8.7 to 75.8 mg/g. However, as the initial concentration of the solution continues to increase, the adsorption capacity reaches 133.4 mg/g at 500 mg/L, and the removal efficiency is as low as 23.1%. This may be due to adsorption saturation of QS-CTS@ZVI. After saturation, no additional
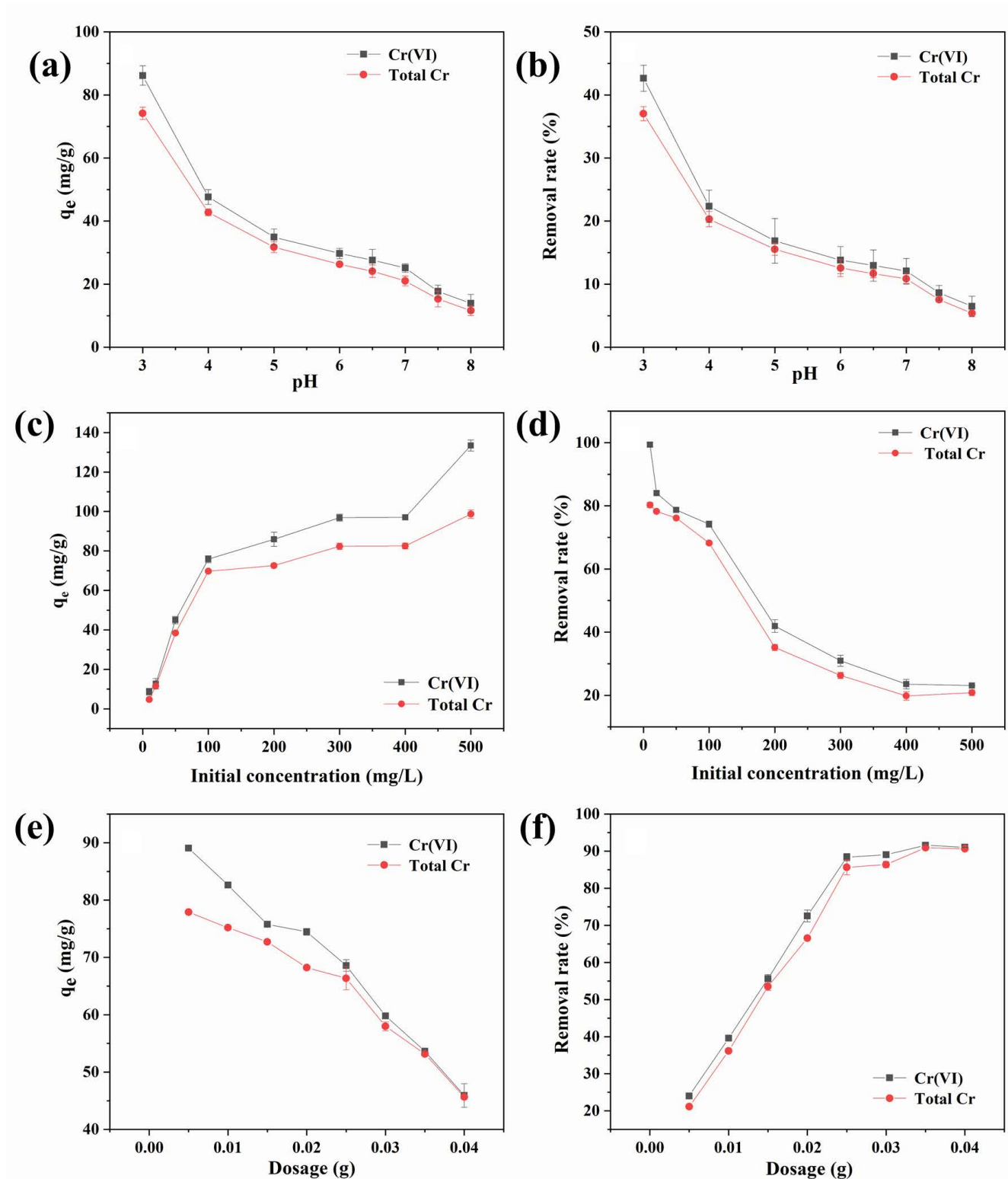
Fig. 5. Effect of initial pH on the (a) equilibrium adsorption capacity and (b) rates of Cr(VI) and total Cr removal by QS-CTS@ZVI (adsorption conditions: 200 mg/L, dosage 0.01 g, 25°C, 5 h); effect of initial concentration on the (c) equilibrium adsorption capacity and (d) rates of Cr(VI) and total Cr removal by QS-CTS@ZVI (adsorption conditions: pH 3, dosage 0.01 g, 25°C, 5 h); dosage effect on the (e) equilibrium adsorption capacity and (f) rates of Cr(VI) and total Cr removal by QS-CTS@ZVI (adsorption conditions: pH 3, 200 mg/L, 25°C, 5 h).

Cr(VI) can be removed. When the initial Cr(VI) concentration is greater than 100 mg/L, the adsorption capacity of QS-CTS@ZVI does not significantly change. This is because the increased abundance of Cr(VI) ions leads to greater competition with the active sites on the adsorbent surface. Too much Cr(VI) in the solution can inhibit the activity of some ZVI powders [54]. At the same time, when the concentration of Cr(VI) is high, a large amount of Cr(VI) is reduced to Cr(III), increasing the combined amount of Cr(III)-Fe(III) oxyhydroxide on the ZVI powder and forming a passivation layer. The main component of the passivation layer is $Cr_{0.667}Fe_{0.333}OOH$ or $Cr_{0.667}Fe_{0.333}(OH)_3$. This also causes the amount of adsorbent material to change slowly. Most of the generated Cr(III) is soluble in water, and a small amount is adsorbed by QS-CTS@ZVI, making the total Cr adsorption lower than the Cr(VI) adsorption.

3.6. Effect of QS-CTS@ZVI dosage

As shown in Fig. 5f, when the dose of QS-CTS@ZVI gradually increases from 0.005 to 0.04 g/L, the removal rate of Cr(VI) increases from 24.0% to 91.6%. With the increase in the QS-CTS@ZVI dosage, the adsorption rate of the coating material for Cr(VI) increases, but an opposite change in the equilibrium adsorption amount of QS-CTS@ZVI is observed (Fig. 5e). In the reaction system, the mass of the QS-CTS@ZVI coating material increases, improving the total number of adsorption sites on the surface of QS-CTS@ZVI and increasing the removal rate of Cr(VI). When the dosage of QS-CTS@ZVI reaches a certain amount, the removal rate of Cr(VI) solution by the adsorbent reaches a certain value and tends to stabilize, resulting in a low content of

Cr(VI) in the solution and the inability to provide a high driving force for diffusion into the adsorbent. However, at this time, some adsorbents still have an excessive number of unoccupied adsorption active sites, so the removal rate of Cr(VI) slightly decreases when the dosage is too large. This indicates that suitable active sites and Cr(VI) content are the key to improving the Cr(VI) removal efficiency. ZVI powder had a certain degree of agglomeration. Loading ZVI with CTS significantly improves the agglomeration of ZVI and increases its antioxidant capacity, and on the surface of the material, ZVI is more likely to react with the negatively charged Cr(VI) adsorbed by CTS and reduce it to Cr(III), which improves the efficiency of Cr(VI) removal by ZVI [20,42,55]. When the dosage of the coating material is 0.035~0.04 g, the removal efficiency of Cr(VI) and total Cr remains above 90%. A greater QS-CTS@ZVI content leads to a greater probability of contact between ZVI and Cr(VI) and a stronger reduction effect. ZVI reduces Cr(VI) to Cr(III), and both Cr(VI) and Cr(III) can be adsorbed and removed by CTS. In addition, the ZVI powder in QS-CTS@ZVI may be oxidized during the adsorption process, but increasing the dosage objectively increases the contents of ZVI and CTS; therefore, the reduction effect and the active adsorption sites in the solution are enhanced. The number of sites increases, and the removal efficiency of Cr(VI) and total Cr increases (with a dosage greater than 0.025 g). Fig. 5e shows that there is a certain difference between the adsorption capacities for Cr(VI) and total Cr. Under the same conditions, the adsorption capacity for Cr(VI) is higher than that for total Cr because the Cr(III) generated by reduction of Cr(VI) is not completely adsorbed by the coating material, and part of the Cr(III) is dissolved in the reaction solution.
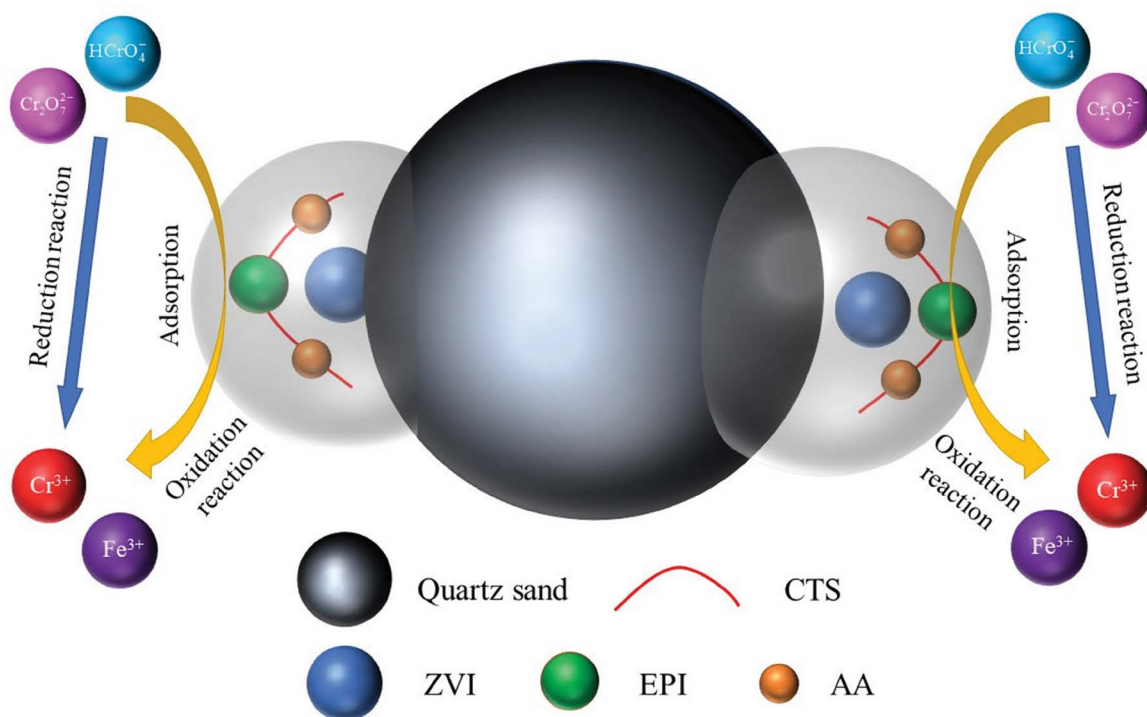

Fig. 6. Possible Cr(VI) removal mechanism of QS-CTS@ZVI.

3.7. Effect of coexisting ions

When QS-CTS@ZVI coexists with NaCl, CaCl$_2$ and MgCl$_2$, the adsorption capacity of QS-CTS@ZVI for Cr(VI) is weakened to varying degrees. This may be because the ZVI powder contained in QS-CTS@ZVI consumes H$^+$ in the solution during the reaction with Cr(VI), and the pH of the whole reaction system gradually increases during the reaction. In this case, Fe(OH)$_3$, Cr(OH)$_3$ or Fe(III)-Cr(III) co-precipitates are formed on the surface of QS-CTS@ZVI [56], hindering adsorption on QS-CTS@ZVI and reduction of Cr(VI) and resulting in a decreased adsorption capacity of the coating material. However, the degree of weakening is small, and electrostatic repulsion between the cations and adsorbents may be present, maintaining the availability of the adsorption sites of the adsorbent for Cr(VI).

The negative effect of anions (SO$_4^{2-}$, H$_2$PO$_4^-$, HCO$_3^-$, PO$_3^{3-}$) on Cr(VI) adsorption is also clear. SO$_4^{2-}$ has the greatest interference in the adsorption of Cr(VI) and total Cr, followed by HCO$_3^-$. This is because anions such as SO$_4^{2-}$ and HCO$_3^-$ in the solution compete with Cr(VI) on the adsorbent (mainly in the form of HCrO$_4^{2-}$ and Cr$_2$O$_7^{2-}$). However, SO$_3^{2-}$ significantly promotes the adsorption of Cr(VI). After SO$_3^{2-}$ is added to the solution, the adsorption amount of QS-CTS@ZVI is 41.9 mg/g higher than that for the blank solution. SO$_3^{2-}$ is more difficult to oxidize in an environment with higher H$^+$ content; thus, the probability of a reduction reaction between QS-CTS@ZVI and Cr(VI) increases, and Cr(VI) is reduced to Cr(III). H$^+$ is also combined with −NH$_2$ in QS-CTS@ZVI to generate positively charged NH$_3^+$, enhancing the electrostatic attraction between the compounds and achieving successful removal of Cr(VI).

3.8. Cyclic adsorption of QS-CTS@ZVI

The removal effect of QS-CTS@ZVI on Cr(VI) is shown in Fig. 4f. After three desorption cycles, the trend of Cr(VI) adsorption by QS-CTS@ZVI changes little, but the removal effect is small (6.85 mg/g) and in the normal range. With three cyclic adsorption experiments, the removal rate of QS-CTS@ZVI is approximately 80%. The above data show that QS-CTS@ZVI shows a good ability to remove Cr(VI), as well as an excellent reuse performance.

3.9. Mechanisms of Cr(VI) removal by QS-CTS@ZVI

Most Cr(VI) in groundwater exists in the form of Cr$_2$O$_7^{2-}$ and HCrO$_4^-$ [57]. The synthetic material is prepared from ZVI-coated QS after loading CTS, and the iron powder is completely wrapped by CTS. When Cr(VI) is in contact with the material, it binds to the abundant binding sites of CTS on the surface of the material, the ZVI inside the material reduces it to Cr(III), and the ZVI is oxidized to Fe(III). During the treatment, the modified CTS plays the role of an adsorbent, Cr(VI) and Cr(III) play a supporting role after the adsorption treatment, and the wrapped quartz sand also plays a supporting role.

4. Conclusion

In this study, the effects of the reaction time, reaction temperature, initial solution pH, initial Cr(VI) concentration,

adsorbent dosage, interference ions and adsorption cycle on the adsorption of Cr(VI) and total Cr by QS-CTS@ZVI were described. The results showed that for a ZVI:CTS ratio of 1:1 (m:m), a QS:ZVI ratio of 1:2 (m:m), a pH of 3, t = 5 h, an initial Cr(VI) concentration of 200 mg/L, a QS-CTS@ZVI dosage of 3.5 g/L, and T = 25°C, the efficiencies of Cr(VI) and total Cr removal by QS-CTS@ZVI were 91.6% and 90.9%, respectively, and an increase in the initial concentration or temperature was conducive to improving the equilibrium adsorption capacity of QS-CTS@ZVI. The pH has a strong influence on the adsorption by the modified material, with the best adsorption capacity obtained under acidic conditions, and the cyclic adsorption performance is good. In particular, the coexistence of SO$_4^{2-}$ and water can significantly inhibit the Cr(VI) adsorption and removal processes. QS-CTS@ZVI performs well in removal of Cr(VI) in an acidic environment, realizes cyclic adsorption, effectively reduces the total Cr content in a water body after adsorption treatment and effectively eliminates Cr pollution after treatment. Thus, QS-CTS@ZVI has great prospects for application in PRB dielectric materials.

Author contributions

Jianlei Gao: experimental design, writing-review and editing, resources, supervision, funding acquisition, project administration, revision. Zixu Zhao and Yu Wang: investigation, data analysis, writing-original draft, revision. Yixin Yan: data analysis, writing-original draft, writing-review & editing, supervision, revision. Mengyuan Feng: writing-review, editing, revision. Jing Wang: revision.

Declaration of competing interests

No conflict of interest exists in the submission of this manuscript, and the manuscript has been approved by all authors for publication.

Acknowledgment

References

[1] I. Maamoun, O. Eljamal, O. Falyouna, R. Eljamal, Y. Sugihara, Multi-objective optimization of permeable reactive barrier design for Cr(VI) removal from groundwater, Ecotoxicol. Environ. Saf., 200 (2020) 110773, doi: 10.1016/j.ecoenv.2020.110773.

[2] H. Tian-Pei, X. Ying, P. Jie-Ru, C. Zhi, L.I. Li-Fen, X.U. Lei, Z. Ling-Ling, G. Xiong, Aerobic Cr(VI) reduction by an indigenous soil isolate *Bacillus thuringiensis* BRC-ZYR2, Pedosphere, 24 (2014) 652–661.

[3] F. Fu, J. Ma, L. Xie, B. Tang, W. Han, S. Lin, Chromium removal using resin supported nanoscale zero-valent iron, J. Environ. Manage., 128 (2013) 822–827.

[4] E. Brasili, I. Bavasso, V. Petruccelli, G. Vilardi, A. Valletta, C. Dal Bosco, A. Gentili, G. Pasqua, L. Di Palma, Remediation of hexavalent chromium contaminated water through zero-valent iron nanoparticles and effects on tomato plant growth performance, Sci. Rep.-UK, 10 (2020) 1920, doi: 10.1038/s41598-020-58639-7.

[5] G. Vilardi, J. Rodriguez-Rodriguez, J. Miguel Ochando-Pulido, L. Di Palma, N. Verdone, Fixed-bed reactor scale-up and

modelling for Cr(VI) removal using nano iron-based coated biomass as packing material, Chem. Eng. J., 361 (2019) 990–998.

[6] S. Lou, S. Liu, C. Dai, A. Tao, B. Tan, G. Ma, R. Chalov, S. Chalov, Heavy metal distribution and groundwater quality assessment for a coastal area on a Chinese Island, Pol. J. Environ. Stud., 26 (2017) 733–745.

[7] C. Qian, W. Zhang, Progress of application of PRB reaction medium materials in remediation of contaminated groundwater, Environ. Eng., 36 (2018) 1–5, 11.

[8] M.M. Scherer, S. Richter, R.L. Valentine, P.J.J. Alvarez, Chemistry and microbiology of permeable reactive barriers for *in situ* groundwater clean-up, Crit. Rev. Microbiol., 26 (2008) 221–264.

[9] R. Thiruvenkatachari, S. Vigneswaran, R. Naidu, Permeable reactive barrier for groundwater remediation, J. Ind. Eng. Chem., 14 (2008) 145–156.

[10] W.K. Walter, U.S. EPA Field Applications of In Situ Remediation Technologies: Permeable Reactive Barriers, EPA, Washington, 1999.

[11] F. Obiri-Nyarko, S.J. Grajales-Mesa, G. Malina, An overview of permeable reactive barriers for in situ sustainable groundwater remediation, Chemosphere, 111 (2014) 243–259.

[12] H. Dong, L. Li, Y. Lu, Y. Cheng, Y. Wang, Q. Ning, B. Wang, L. Zhang, G. Zeng, Integration of nanoscale zero-valent iron and functional anaerobic bacteria for groundwater remediation: a review, Environ. Int., 124 (2019) 265–277.

[13] R.W. Gillham, S.F. Ohannesin, enhanced degradation of halogenated aliphatics by zero-valent iron, Groundwater, 32 (1994) 958–967.

[14] J. Klausen, P.J. Vikesland, T. Kohn, D.R. Burris, W.P. Ball, A.L. Roberts, Longevity of granular iron in groundwater treatment processes: solution composition effects on reduction of organohalides and nitroaromatic compounds, Environ. Sci. Technol., 37 (2003) 1208–1218.

[15] P. Lacina, V. Dvorak, E. Vodickova, P. Barson, J. Kalivoda, S. Goold, The application of nano-sized zero-valent iron for in situ remediation of chlorinated ethylenes in groundwater: a field case study, Water Environ. Res., 87 (2015) 326–333.

[16] R.M. Powell, R.W. Puls, S.K. Hightower, D.A. Sabatini, Coupled iron corrosion and chromate reduction: mechanisms for subsurface remediation, Environ. Sci. Technol., 29 (1995) 1913–1922.

[17] C. Kantar, C. Ari, S. Keskin, Z.G. Dogaroglu, A. Karadeniz, A. Alten, Cr(VI) removal from aqueous systems using pyrite as the reducing agent: batch, spectroscopic and column experiments, J. Contam. Hydrol., 174 (2015) 28–38.

[18] R.T. Wilkin, R.W. Puls, G.W. Sewell, Long-term performance of permeable reactive barriers using zero-valent iron: geochemical and microbiological effects, Groundwater, 41 (2003) 493–503.

[19] Z. Wang, G. Chen, X. Wang, S. Li, Y. Liu, G. Yang, Removal of hexavalent chromium by bentonite supported organosolv lignin-stabilized zero-valent iron nanoparticles from wastewater, J. Cleaner Prod., 267 (2020) 122009, doi: 10.1016/j.jclepro.2020.122009.

[20] M. Cai, J. Zeng, Y. Chen, P. He, F. Chen, X. Wang, J. Liang, C. Gu, D. Huang, K. Zhang, M. Gan, J. Zhu, An efficient, economical, and easy mass production biochar supported zero-valent iron composite derived from direct-reduction natural goethite for Cu(II) and Cr(VI) remove, Chemosphere (Oxford), 285 (2021) 131539, doi: 10.1016/j.chemosphere.2021.131539.

[21] F. Zhu, X. Tan, W. Zhao, L. Feng, S. He, L. Wei, L. Yang, K. Wang, Q. Zhao, Efficiency assessment of ZVI-based media as fillers in permeable reactive barrier for multiple heavy metal-contaminated groundwater remediation, J. Hazard. Mater., 424 (2022) 127605, doi: 10.1016/j.jhazmat.2021.127605.

[22] C. Wang, Z. Xu, G. Ding, X. Wang, M. Zhao, S.S.H. Ho, Y. Li, Comprehensive study on the removal of chromate from aqueous solution by synthesized kaolin supported nanoscale zero-valent iron, Desal. Water Treat., 57 (2015) 5065–5078.

[23] S. Peng, H. Meng, Y. Ouyang, J. Chang, Nanoporous magnetic cellulose– chitosan composite microspheres: preparation, characterization, and application for Cu(II) adsorption, Ind. Eng. Chem. Res., 53 (2014) 2106–2113.

[24] E.I. Rabea, M.E.T. Badawy, C.V. Stevens, G. Smagghe, W. Steurbaut, Chitosan as antimicrobial agent: applications and mode of action, Biomacromolecules, 4 (2003) 1457–1465.

[25] R. Zhao, X. Zheng, J. Ren, X. Tang, Y. Long, H. Zheng, Research progress on the modification of chitosan by cross-linking and grafting, Polym. Bull., (2019) 43–50.

[26] H.M. Ibrahim, M. Mostafa, N.G. Kandile, Potential use of N-carboxyethylchitosan in biomedical applications: preparation, characterization, biological properties, Int. J. Biol. Macromol., 149 (2020) 664–671.

[27] J. Dai, H. Yan, H. Yang, R. Cheng, Simple method for preparation of chitosan/poly(acrylic acid) blending hydrogel beads and adsorption of copper(II) from aqueous solutions, Chem. Eng. J., 165 (2010) 240–249.

[28] Q. Song, C. Wang, Z. Zhang, J. Gao, Adsorption of Cu(II) and Ni(II) using a novel xanthated carboxymethyl chitosan, Sep. Sci. Technol., 49 (2014) 1235–1243.

[29] X. Wang, Y. Zheng, A. Wang, Fast removal of copper ions from aqueous solution by chitosan-*g*-poly(acrylic acid)/attapulgite composites, J. Hazard. Mater., 168 (2009) 970–977.

[30] Y. Lin, Y. Hong, Q. Song, Z. Zhang, J. Gao, T. Tao, Highly efficient removal of copper ions from water using poly(acrylic acid)-grafted chitosan adsorbent, Colloid Polym. Sci., 295 (2017) 627–635.

[31] Y.S. Ho, G. McKay, Sorption of dye from aqueous solution by peat, Chem. Eng. J., 70 (1998) 115–124.

[32] H. Ge, H. Chen, S. Huang, Microwave preparation and properties of O-crosslinked maleic acyl chitosan adsorbent for Pb^{2+} and Cu^{2+}, J. Appl. Polym. Sci., 125 (2012) 2716–2723.

[33] G. Vilardi, Mathematical modelling of simultaneous nitrate and dissolved oxygen reduction by Cu-nZVI using a bi-component shrinking core model, Powder Technol., 343 (2019) 613–618.

[34] V.V. Thekkae Padil, J. Filip, K.I. Suresh, S. Wacławek, M. Černík, Electrospun membrane composed of poly[acrylonitrile-co-(methyl acrylate)-co-(itaconic acid)] terpolymer and ZVI nanoparticles and its application for the removal of arsenic from water, RSC Adv., 6 (2016) 110288–110300.

[35] P.B. Vilela, C.A. Matias, A. Dalalibera, V.A. Becegato, A.T. Paulino, Polyacrylic acid-based and chitosan-based hydrogels for adsorption of cadmium: equilibrium isotherm, kinetic and thermodynamic studies, J. Environ. Chem. Eng., 7 (2019) 103327.

[36] N.A. Mohamed, N.A. Abd El-Ghany, Pyromellitimide benzoyl thiourea cross-linked carboxymethyl chitosan hydrogels as antimicrobial agents, Int. J. Polym. Mater. Polym. Biomater., 66 (2017) 861–870.

[37] T. Liu, B. Li, J. Zhang, L. Zhu, J. Chen, Kinetic studies on the pyrolysis of chitosan and chitin, Food Ferment. Ind., 36 (2010) 32–36.

[38] S. El-Houte, M. El-Sayed Ali, O.T. Sørensen, Dehydration of CuSO$_4$·5H$_2$O studied by conventional and advanced thermal analysis techniques, Thermochim. Acta, 138 (1989) 107–114.

[39] T. Liu, Kinetic studies on the pyrolysis of a water-soluble chitosan, Univ. Nat. Sci., 46 (2012) 65–70.

[40] H.F.G. Barbosa, D.S. Francisco, A.P.G. Ferreira, É.T.G. Cavalheiro, A new look towards the thermal decomposition of chitins and chitosans with different degrees of deacetylation by coupled TG-FTIR, Carbohydr. Polym., 225 (2019) 115232, doi: 10.1016/j.carbpol.2019.115232.

[41] C. Xu, W. Yang, W. Liu, H. Sun, C. Jiao, A. Lin, Performance and mechanism of Cr(VI) removal by zero-valent iron loaded onto expanded graphite, J. Environ. Sci.-China, 67 (2018) 14–22.

[42] Y. Gong, L. Gai, J. Tang, J. Fu, Q. Wang, E.Y. Zeng, Reduction of Cr(VI) in simulated groundwater by FeS-coated iron magnetic nanoparticles, Sci. Total Environ., 595 (2017) 743–751.

[43] A.J. Varma, S.V. Deshpande, J.F. Kennedy, Metal complexation by chitosan and its derivatives: a review, Carbohydr. Polym., 55 (2004) 77–93.

[44] G. Vilardi, B. De Caprariis, M. Stoller, L. Di Palma, N. Verdone, Intensified water denitrification by means of a spinning disk reactor and stirred tank in series: kinetic modelling and computational fluid dynamics, J. Water Process Eng., 34 (2020) 101147, doi: 10.1016/j.jwpe.2020.101147.

[45] T. Yoadsomsuay, N. Grisdanurak, C.H. Liao, Influence of chitosan on modified nanoscale zero-valent iron for arsenate removal, Desal. Water Treat., 57 (2016) 17861–17869.

[46] H. Chen, J. Dou, H. Xu, The effect of low-molecular-weight organic-acids (LMWOAs) on treatment of chromium-contaminated soils by compost-phytoremediation: kinetics of the chromium release and fractionation, J. Environ. Sci.-China, 70 (2018) 45–53.

[47] Z. Yu, L. Hu, I.M.C. Lo, Transport of the arsenic(As)-loaded nano zero-valent iron in groundwater-saturated sand columns: roles of surface modification and As loading, Chemosphere, 216 (2019) 428–436.

[48] Y. Wen, Z. Tang, Y. Chen, Y. Gu, Adsorption of Cr(VI) from aqueous solutions using chitosan-coated fly ash composite as biosorbent, Chem. Eng. J., 175 (2011) 110–116.

[49] T. Liu, I.M.C. Lo, Influences of humic acid on Cr(VI) removal by zero-valent iron from groundwater with various constituents: implication for long-term PRB performance, Water, Air, Soil Pollut., 216 (2011) 473–483.

[50] L. Yan, M. Liu, X. Hu, Removal of Cr(VI) in soil by chitosan stabilized nanoscale zero iron, Nat. Sci. Ed., 22 (2016) 203–210.

[51] T. Mpouras, A. Polydera, D. Dermatas, N. Verdone, G. Vilardi, Multi wall carbon nanotubes application for treatment of Cr(VI)-contaminated groundwater; modeling of batch & column experiments, Chemosphere, 269 (2021) 128749, doi: 10.1016/j.chemosphere.2020.128749.

[52] H. Dong, J. Deng, Y. Xie, C. Zhang, Z. Jiang, Y. Cheng, K. Hou, G. Zeng, Stabilization of nanoscale zero-valent iron (nZVI) with modified biochar for Cr(VI) removal from aqueous solution, J. Hazard. Mater., 332 (2017) 79–86.

[53] J. Liu, T. Mwamulima, Y. Wang, Y. Fang, S. Song, C. Peng, Removal of Pb(II) and Cr(VI) from aqueous solutions using the fly ash-based adsorbent material-supported zero-valent iron, J. Mol. Liq., 243 (2017) 205–211.

[54] L. Wu, L. Liao, G. Lv, F. Qin, Y. He, X. Wang, Micro-electrolysis of Cr(VI) in the nanoscale zero-valent iron loaded activated carbon, J. Hazard. Mater., 254–255 (2013) 277–283.

[55] L. Liu, L. Liang, Y. Shi, X. Wang, K. Feng, S. Wang, Sulfidation enhanced Cr(VI) reduction by zero-valent iron under different environmental conditions: a mechanistic study, J. Agro-Environ. Sci., 40 (2021) 1079–1087.

[56] M. Hou, H. Wan, T. Liu, Y. Fan, X. Liu, X. Wang, The effect of different divalent cations on the reduction of hexavalent chromium by zero-valent iron, Appl. Catal., B, 84 (2008) 170–175.

[57] H. Zhang, R. Xiao, R. Li, A. Ali, A. Chen, Z. Zhang, Enhanced aqueous Cr(VI) removal using chitosan-modified magnetic biochars derived from bamboo residues, Chemosphere, 261 (2020) 127694, doi: 10.1016/j.chemosphere.2020.127694.

Supporting information

Fig. S1a and b shows that the removal effect of Cr(VI) under acidic conditions is much higher than that under neutral conditions, and the addition of zero-valent iron powder has an effect on the removal of Cr(VI); however, the impact is weak. When the pH value is 3, the removal of Cr(VI) by chitosan (CTS) depends on the electrostatic attraction and chelation between the protonated group and Cr(VI), and this effect is greatly weakened under neutral conditions, so the removal effect of SA-CTS@ZVI is greatly reduced. In addition, although the zero-valent iron powder generates Fe(III) and Fe(II) under acidic conditions, which has a reducing effect on Cr(VI), if the content of zero-valent iron powder is too high, it will reduce CTS and zero-valent iron. The steric hindrance between the powders and the agglomeration of the zero-valent iron powder itself will affect the removal effect. The results in Fig. S1b show that the ratio of quartz sand to zero-valent iron powder in the range of 1:2~1:4 has very little

Table S1
Parameters of intraparticle diffusion model

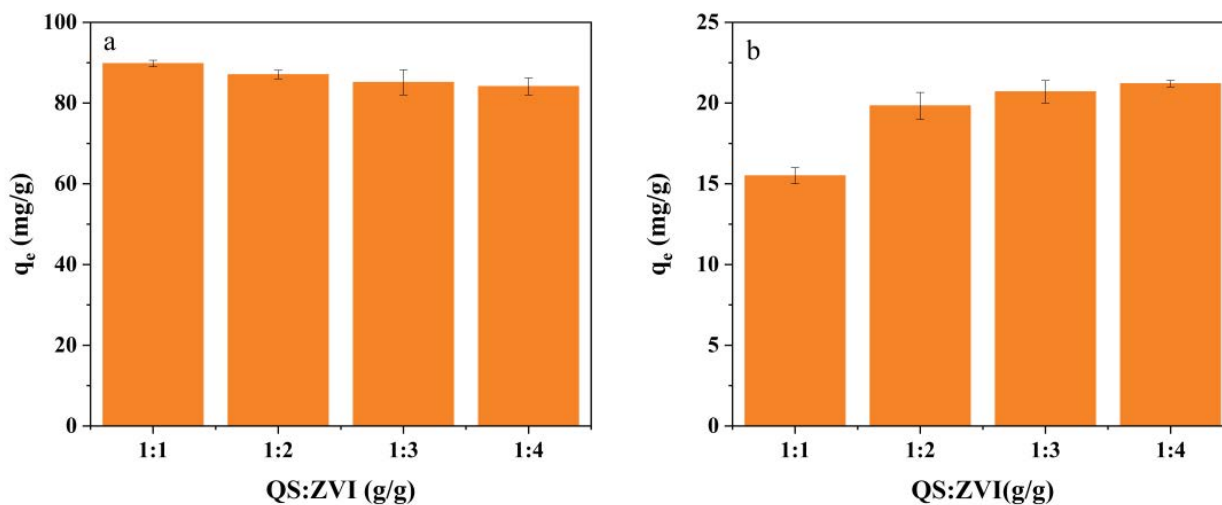| Concentration of Cr(VI) (mg/L)	100	200	300
C_i (mg/g)	28.44814	87.13499	85.99219
	84.47967	89.17238	89.77556
	81.09584	86.80589	89.43121

Fig. S1. Effect of ZVI content on Cr(VI) adsorption performance (a) pH of 3 and (b) pH of 6.

Table S2
QS-CTS@ZVI dynamic parameters

Kinetic model					Parameter	
	Concentration of Cr(VI)	$q_{e(cal)}$ (mg/g)	k_1 (min^{-1})	R^2		$q_{e(exp)}$ (mg/g)
Pseudo-first-order	100 mg/L	18.64168123	0.00516	0.68947		86.61865
	200 mg/L	30.76414843	0.0072	0.92086		87.23819
	300 mg/L	37.10530681	0.00707	0.86182		115.34499
	Concentration of Cr(VI)	$q_{e(cal)}$ (mg/g)	k_2 (min^{-1})	R^2		$q_{e(exp)}$ (mg/g)
Pseudo-second-order	100 mg/L	87.33624	0.001408	0.99963		86.61865
	200 mg/L	89.52551	0.000749	0.99883		91.91176
	300 mg/L	119.3317	0.000547	0.99882		115.34499

Table S3
QS-CTS@ZVI isothermal model parameters

		Parameter		
	T (°C)	K_L (L/mg)	R^2	$q_{e(cal)}$ (mg/g)
Langmuir	293 K	0.02228	0.98396	114.8106
	298 K	0.029949	0.98769	120.3369
	303 K	0.033974	0.99411	123.6094
	T (°C)	K_L (L/mg)	R^2	$1/n$
Freundlich	293 K	34.40646	0.95129	0.18266
	298 K	44.44675	0.94317	0.15227
	303 K	45.72566	0.9869	0.15533

difference in the removal effect of Cr(VI). Therefore, in subsequent processes of preparing SA-CTS@ZVI, a ratio of 1:2 between quartz sand and zero-valent iron powder should be maintained.

From the comparison in Table S2, it can be seen that at the initial concentrations of 100, 200 and 300 mg/L, the maximum adsorption capacities of 87.3, 91.1 and 119.3 mg/g simulated by quasi-second-order kinetics are very close to those obtained by experiments of 86.6, 87.2 and 115.3 mg/g. In the fitting parameters of the second-order reaction kinetics, the value of k_2 decreased from 0.0014 to 0.00055 min^{-1} as the concentration increased from 100 to 300 mg/L. This shows that the active sites on the surface of quartz sand chitosan zero-valent iron are occupied by Cr(VI) at high concentrations, and the energy consumed by adsorption increases.